INFLUENCE OF GEOMETRY ON GMI EFFECT OF Co-BASED MAGNETIC COMPOSITE MICROWIRES

F.X. Qin[1], N.Pankratov[1], H.X.Peng[1], J. Tang[2], L.V. Panina[3].
[1]Advanced Composite Center for Innovation and Science, Department of Aerospace Engineering, University of Bristol, University Walk, Bristol, BS8 1TR, UK
[2]1D Nanomaterials Group, National Institute for Material Science, 1-2-1 Sengen, Tsukuba, Ibaraki 305-0047, JAPAN
[3]School of computing, Communication and Electronics, University of Plymouth, Drake Circus, Plymouth, Devon, PL4 8AA, UK
Faxiang.qin@bris.ac.uk

SUMMARY

The influence of varying geometrical factors on the magnetoimpedance (MI) effect in amorphous glass-coated CoFeNiBSiMo microwires has been investigated. The wire geometry and quality of surfaces were deduced from SEM micrographs of the microwires. MI characteristics are influenced by the wire geometry due to metal-glass adhesion, frozen-in stress distribution, and magnetostatic interactions. We found that increasing *t* results in increase in the coercivity and anisotropy. In the range of frequencies investigated (0.1 – 10 MHz), the magnitude of the MI effect may greatly increase as *h* decreases from 17.40 to 5.33 even if the anisotropy is strongly increased.

Keywords: Composite microwires; Magnetic property; MI; Microscopy; Internal stress.

INTRODUCTION

Glass coated amorphous wires of Co-based composition have a unique circular magnetic anisotropy due to coupling between negative magnetostriction and frozen-in stress. Such anisotropy is important to realize large and sensitive magnetoimpedance (MI) effect for applications in miniature magnetic sensors and sensing composite materials[1]. The MI effect refers to a strong variation in the high frequency impedance of a magnetic conductor subjected to a small dc magnetic field, which is observed at frequencies when the skin effect is strong. According to the frequency range, it can be classified into three regions[2-6]: (i) At relatively low-frequency range of (hundred kHz to MHz), the change of impedance is mainly due to circular domain wall dynamics; (ii) At medium frequency range from few MHz to hundred MHz, the wall motion is strongly damped and the rotational processes mainly contribute to the ac permeability and impedance change; (iii) At higher frequencies beyond the ferromagnetic resonance

(GHz range), the rotational permeability becomes less sensitive to the field and the impedance change is related with the reorientation of the dc magnetization. In all three cases, the characteristic field of the impedance change is defined by the value and distribution of the circular anisotropy. In this work, we make further progress in tailoring a circular anisotropy and impedance by changing the wire geometry. The possibility of obtaining larger MI ratios by increasing the anisotropy is demonstrated which contrasts with many previous results [7, 8].

Glass-coated amorphous wires consist of an amorphous metallic core and glass coat of the order of several microns. The function of the glass insulation is twofold: one is that it can protect the metallic core from oxidation and make it possible to fabricate the microwire of very small diameter; The other is that the glass coat provides more freedom degree to control the magnetic structure and properties of the wires. This is because the effective magnetic anisotropy defining the wire magnetic structure depends on wire geometry. In amorphous wires, the anisotropy is dominated by magnetoelastic contribution coupled with internal stresses, induced during a fast solidification of the glass-coat and metallic core having different thermal expansion coefficients. Then, the resulting anisotropy is strongly dependent on the wire geometry including the metal diameter d, glass-coat thickness t, and metal-to-glass ratio h.

EXPERIMENTAL DETAILS

Three CoFeNiBSiMo wires of similar composition but different geometry produced by a modified Taylor-Ulitovski process[9, 10] were investigated. Scanning electron microscopes (SEM JEOL JSM-6500) was used for examining the samples prepared by mechanical polishing, which are carried out using the automatic polishing machine with the fixed force, time and procedure. Their geometrical parameters are summarized in Table 1.

Table 1 The geometrical parameters, calculated radial frozen-in stress (σ) in radial (σ_{rr}), azimuthal ($\sigma_{\phi\phi}$) and axial direction (σ_{zz}) and maximum GMI ($[\Delta Z/Z]_{max}$) at 4 MHz.

Sample	d, μm	t, μm	h	σ,MPa		$[\Delta Z/Z]_{max}$ (%)
				$\sigma_{rr},\sigma_{\phi\phi}$	σ_{zz}	
1	17.4	1	17.40	25.81	52.82	65.31
2	17.6	3.3	5.33	86.86	185.81	114.23
3	9.9	1.9	5.21	88.94	190.51	29.08

These microwires possess good soft magnetic properties owing to the nearly zero and negative magnetostriction ($\lambda \sim -10^{-7}$). The magnetoimpedance was measured by a HP8753E network analyzer in the frequency range of 500kHz - 10 MHz. The measuring cell with a microwire was placed in the solenoid producing DC fields up to 30Oe along

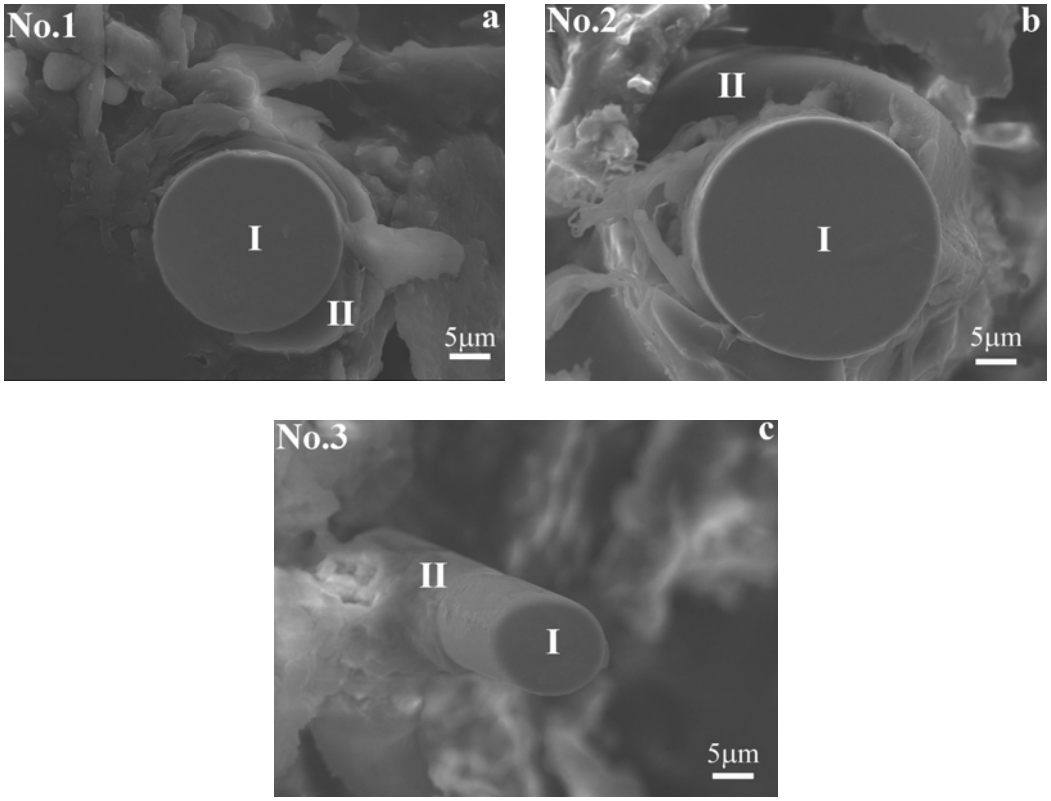

Fig. 1 Cross-section SEM images of as prepared microwires at 3000×: $Fe_{3.85}Co_{67.05}Ni_{1.44}B_{11.53}Si_{14.47}Mo_{1.66}$ (a); $Fe_4Co_{68.7}Ni_1B_{13}Si_{11}Mo_{2.3}$ (b); $Fe_{3.84}Co_{67.05}Ni_{1.44}B_{11.51}Si_{14.47}Mo_{1.69}$ (c).

the wire axis and vertical to the geomagnetic field. S11 port of the two-port network was applied to pick up the signal of output power and the S-parameter was then converted to the impedance by program calculation. The magnetoimpedance ratio ΔZ/Z is defined as:

$$\frac{\Delta Z}{Z}(\%) = \frac{Z(H) - Z(H_{\max})}{Z(H_{\max})} \times 100\% \tag{1}$$

where $Z(H)$ and $Z(H_{\max})$ are the impedance magnetudes of the microwire in the measured external magnetic field and maximum magnetic field to saturate the wire, respectively.

RESULTS AND DISCUSSION

Figure 1 displays the SEM images on the wires of different core diameters and glass-coat thicknesses after carbon-coated on the surfaces. Zone I denotes the metallic core and Zone II represents the glass coat. They are surrounded by the resin used for

preparing the wire samples for observation. It is interesting to find that the sample No.3, which possesses the lowest metal-to-glass ratio (h), exhibits very smooth side surfaces left when the glass-coats fell off. It follows that the condition of the cohesion between glass coat and the metal is likely to be dependent on the value of h. During fabrication, a stress will be imposed to the metallic core from the glass coat. The lower h, which indicates the smaller size difference between metallic core and glass coat, will yield higher stress. Hence, once the external force is applied to the wires, the two layers are very prone to breaking apart, consequently leaving a very smooth surface. With the largest value of h, the cross-section of the glass coat of No.1 can be seen fully covered by resin, suggesting that, after the glass fell off, the surface left is rough enough to allow an inflow and adhesion of resin. The fact that the No.1 wire has the minimum thickness of glass-coat further corroborates the significance of metal-to-glass ratio for the stress at the glass-metal interface. No.2 wire, with the similar metal-to-glass ratio as the No.3 wire, presents a partially resin covered glass-coat surface, can be attributed to its maximum thickness of all.

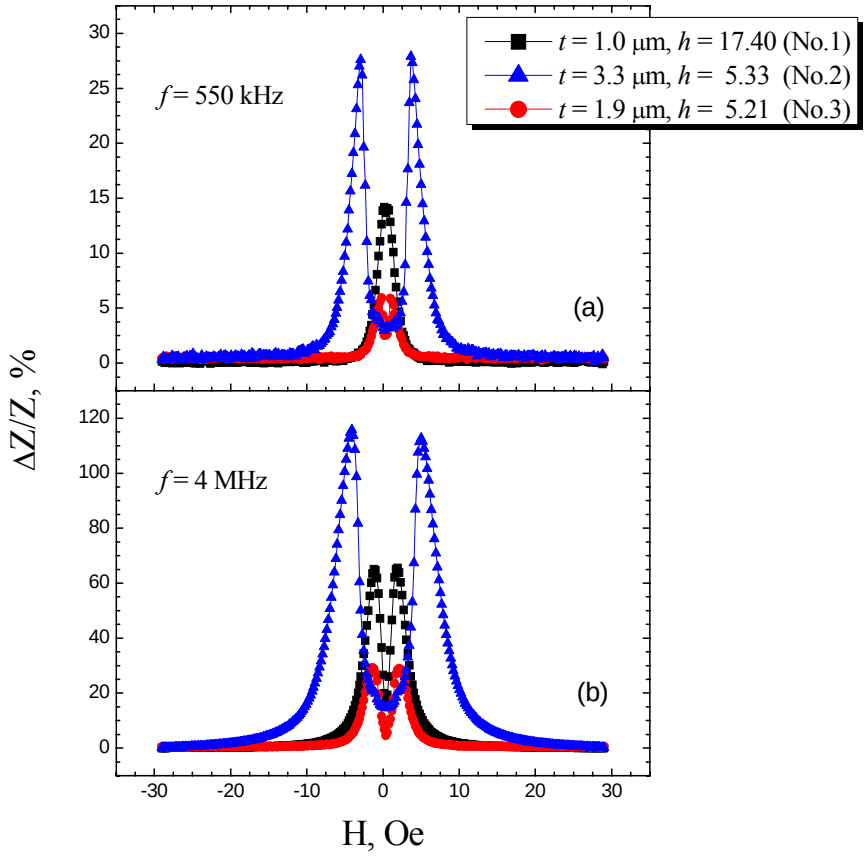

Fig. 2. Magnetic field dependence of GMI ratio (ΔZ/Z) for Samples No.1 (t = 1.0μm, h = 17.40), Samples No.2 (t = 3.3μm, h = 5.33) and Samples No.3 (t = 1.9μm, h = 5.21), taken at representative frequencies f = 550 kHz (a), 4 MHz (b)

A further quantitative elaboration can be found in the calculation of the internal stress

tensor: σ_{rr}, $\sigma_{\phi\phi}$ and σ_{zz} in the radial, azimuthal and axial directions, respectively. We will be restricted to thermoelastic stress and neglect the quenching stress as the latter is typically much smaller [11]:

$$\begin{aligned}
\sigma_{rr} &= \varepsilon E_m k(1-p^2)/\left[(k/4)\left(1-p^2\right)+4p^2/3\right] \\
\sigma_{\phi\phi} &= \sigma_{rr} \\
\sigma_{zz} &= \sigma_{rr}[(k+1)(1-p^2)+2p^2]/[k(1-p^2)+p^2] \\
p &= \frac{h}{h+1} \\
k &= E_g / E_m \\
\varepsilon &= \left(\alpha_m - \alpha_g\right)\left(T^*-T\right)
\end{aligned} \tag{2}$$

where E_g and E_m are the Young's modulus of glass and metal core, respectively. a_m and a_g are the thermal expansion coefficient of metal and glass, respectively. The values of stress, calculated from this equation and the data provided in Ref. [12, 13]， are given in Table 1.

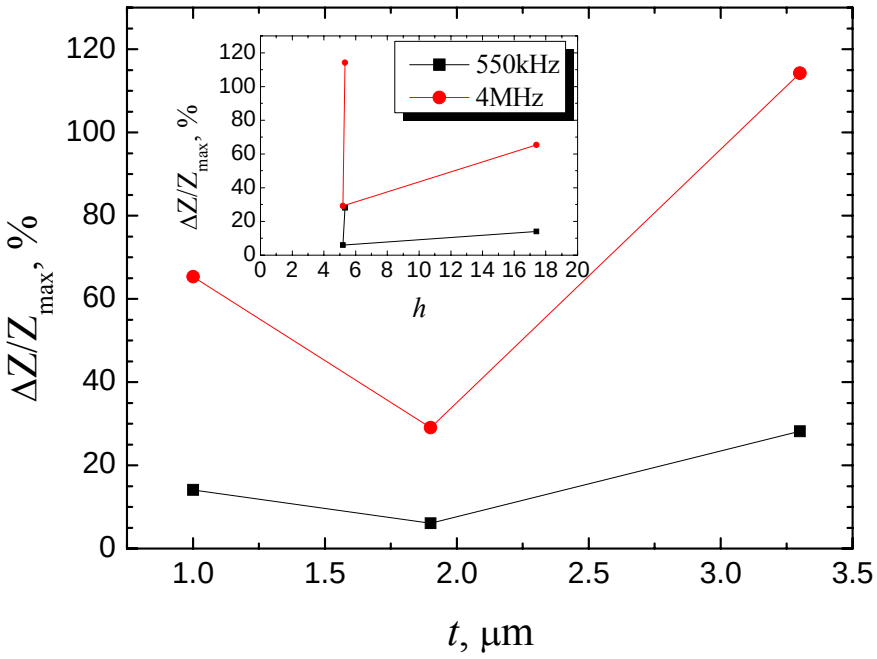

Fig. 3. Glass thickness dependence of maximum MI ratio ($[\Delta Z/Z]_{max}$) at representative frequencies f = 550KHz and 4MHz. The inset shows the metal-to-glass ratio of $[\Delta Z/Z]_{max}$ at the corresponding frequencies.

Figure 2 shows the magnetic field dependence of MI ($\Delta Z/Z$) at representative frequencies f = 550kHz and 4 MHz. It can be observed that the MI curves show a

single-peak feature for $f \leq 550$ kHz and a double-peak feature for $f > 550$ kHz for Sample No.1 ($t = 1.0\mu m$, $h = 17.40$), which could be attributed to domain wall dynamics still essential at this frequency for a wire with the smallest anisotropy. A double-peak feature is observed for samples with larger anisotropy No.2 ($t = 3.3\mu m$, $h = 5.33$) and No.3 ($t = 1.9\mu m$, $h = 5.21$) in the frequency range of 550 kHz – 10 MHz. Noticeably, the height and shape of MI curves vary strongly with the glass thickness (t) and metal-to-glass ratio (h).

To elucidate these intriguing features, we plot in Fig. 3 the t dependence of maximum MI ratio ($[\Delta Z/Z]_{max}$) at $f = 550$kHz and 4MHz. The corresponding h dependence of $[\Delta Z/Z]_{max}$ is also included in inset of Fig. 3. It can be seen that the $[\Delta Z/Z]_{max}$ decreases as the metal-to-glass ratio (h) decreases from $h = 17.40$ to $h = 5.21$. However, the $[\Delta Z/Z]_{max}$ starts to increase strongly from $t = 1.9\mu m$ to $t = 3.3\mu m$ in spite of the increase of h from 5.21 to 5.33. Another noticeable feature is that the magnetic field corresponding to the double-peak position in GMI curves (known as the anisotropy field, H_k) increases from $t = 1.0$ μm to $t = 3.3\mu m$ as shown in Fig. 4 and its inset. In addition, the magnitude of H_k increases with measurement frequency， which may imply a strongly non-uniform stress distribution towards the surface.

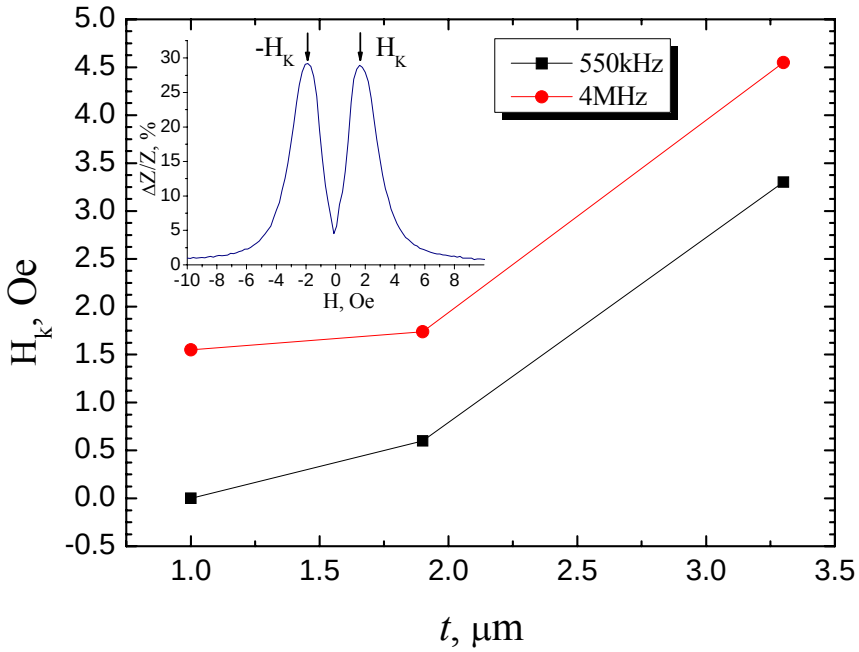

Fig. 4. Glass thickness dependence of the anisotropy field (H_k) determined from the MI peak position as illustrated in the inset of Fig. 4

The sign and magnitude of magnetostriction constant (λ) determines the type of domain structure in the glass-coated microwires [4, 14]. For microwires with positive magnetostriction, the frozen-in stress distribution results in a longitudinal easy axis in the cylindrical core and radial easy axes in the tubular shell. Meanwhile, for microwires

with negative magnetostriction, the axial and radial tensile stresses cause the surface anisotropy to be circular but the anisotropy in the inner area may be still axial due to exchange interaction. Thus, this could lead to the formation of a specific domain structure, which consists of circular domains in the outer shell and axial domains in the inner core[15, 16]. In the present case, the glass-coated Co-rich microwire has a vanishing magnetostriction constant ($\lambda \sim -10^{-7}$). Accordingly, one can expect that the domain structure of this microwire consists of outer shell circular domains and inner core axial domains with the value of the circular anisotropy increasing towards the surface. At lower frequencies, the displacements of the circular domains mainly contribute to the impedance change. The external field gradually magnetizes the wire and eliminates the domain structure, thus removing this mechanism of the magnetic dynamics. This results in a single peak behavior with impedance maximum at zero field. With increasing the frequency, the domain movements are damped and rotational dynamics becomes more important. The rotational permeability reaches a maximum when the external field is nearly the anisotropy field. This leads to a general expectation that these microwires should show a single-peak feature at low frequency but a double-peak feature at high frequency [1,2]. This explains why the MI curve shows a single-peak feature at f = 550 kHz and a double-peak feature at f = 4 MHz for the case of Sample No.1. For the other samples No.2 (t = 3.3μm) and No.3 (t =1.9μm), it is shown that the increase of the glass thickness (t) leads to the increase in the anisotropy, coercivity, and, very probably, circular anisotropy area. Then, the domain dynamics may be already strongly damped at a frequency of 550 kHz, so a single-peak shape in MI plots is not observed with these samples. A strong increase in the MI ratio with sample No.2 (t = 3.3μm) with the highest anisotropy can be explained by better defined circular anisotropy with less deviations of the anisotropy axes from the circular direction. This result differs greatly from those reported in [8] where the wires with smaller anisotropy generated larger MI ratios.

CONCLUSIONS

For amorphous glass-coated Co-rich microwires in the frequency range of 100kHz – 10 MHz, the magnitude and shape of MI curves vary strongly with the glass thickness and metal-to-glass ratio. When t < ~2μm, the metal-to-glass ratio plays a dominating role in deciding the domain structure; when t > ~3μm, the glass-coat thickness became the overriding factor. The calculated residual stress decreases with the metal-to-glass ratio. These results provide further understanding of the correlation between the MI effect and microwire dimensions towards the MI optimization of amorphous glass-coated magnetic microwires.

ACKNOWLEDGEMENTS

FXQ is supported through Overseas Research Students Awards Scheme and University

of Bristol Postgraduate Student Scholarship. HXP would like to acknowledge the financial support from the Engineering and Physical Science Research Council (EPSRC) UK under the Grant No. EP/FO3850X. The authors would also thank Nick Fry for the help with the GMI measurement.

References

1. L. V. Panina, J. Magn. Magn. Mater., 2002. **249**(1-2): p. 278-287.
2. L. V. Panina, K. Mohri, T. Uchiyama, and M. a. B. K. Noda, Magnetics, IEEE Transactions on, 1995. **31**(2): p. 1249-1260.
3. D. P. Makhnovskiy, L. V. Panina, and D. J. Mapps, Phys. Rev. B, 2001. **63**(14): p. 144424--.
4. M.-H. Phan and H.-X. Peng, Prog. Mater Sci., 2008. **53**(2): p. 323--420.
5. A. Yelon, D. Menard, M. Britel, and P. Ciureanu, Appl. Phys. Lett., 1996. **69**(20): p. 3084-3085.
6. S. I. Sandacci, D. P. Makhnovskiy, and L. V. Panina, J. Magn. Magn. Mater., 2004. **272-276**(Part 3): p. 1855--1857.
7. V. Zhukova, A. Chizhik, A. Zhukov, A. Torcunov, V. Larin, and J. Gonzalez, Magnetics, IEEE Transactions on, 2002. **38**(5): p. 3090--3092.
8. V. Zhukova, V. S. Larin, and A. Zhukov, J. Appl. Phys., 2003. **94**(2): p. 1115-1118.
9. G. F. Taylor, Phys. Rev., 1924. **23**(5): p. 655-660.
10. A. V. Ulitovsky, I. M. Maianski, and A. I. Avramenco, Patent No. 128427 (USSR), 15.05.60, Bulletin. No. 10, p. 14.
11. A. V. Torcunov, S. A. Baranov, and V. S. Larin, J. Magn. Magn. Mater., 1999. **196-197**: p. 835-836.
12. A. L. Adenot, S. Deprot, F. Bertin, D. Bois, and O. Acher, J. Magn. Magn. Mater., 2004. **272-276**(Supplement 1): p. E1115-E1116.
13. H. Montiel, G. Alvarez, M. P. Gutierrez, R. Zamorano, and R. Valenzuela, Magnetics, IEEE Transactions on, 2006. **42**(10): p. 3380 - 3382.
14. M. Vazquez and A. Hernando, J. Phys. D: Appl. Phys., 1996. **29**(4): p. 939-949.
15. H. Chiriac, S. Corodeanu, M. Tibu, and T. A. Ovari, Magnetics, IEEE Transactions on, 2007. **43**(6): p. 2977-2979.
16. H. Chiriac, V. Goian, and S. Corodeanu, Magnetics, IEEE Transactions on, 2006. **42**(10): p. 3359-3361.